INORGANIC CHEMISTRY
ACCEPTED MANUSCRIPT

Pt-B system re-visited: Pt_2B, a new structure type of binary borides. Ternary WAl_{12}-type derivative borides.

Oksana Sologub[1,*], Leonid Salamakha[1], Peter Rogl[2], Berthold Stöger[3], Ernst Bauer[1], Johannes Bernardi[4], Gerald Giester[5], Monika Waas[1], Robert Svagera[1]

[1]Institute of Solid State Physics, TU Wien, A-1040 Vienna, Austria

[2]Institute of Materials Chemistry and Research, University of Vienna, A-1090 Vienna, Austria

[3]Institute for Chemical Technologies and Analytics, TU Wien, A-1040 Vienna, Austria

[4]University Service Center for TEM (USTEM), TU Wien, A-1040 Vienna, Austria

[5]Institute of Mineralogy and Crystallography, University of Vienna, A-1090 Vienna, Austria

ABSTRACT

Based on a detailed study applying X-ray single crystal and powder diffraction, DSC and SEM analysis it was possible to resolve existing uncertainties in the Pt-rich section (≥65 at.% Pt) of the binary Pt-B phase diagram above 600°C. The formation of a unique structure has been observed for Pt_2B (X-ray single crystal data: SG *C*2/*m*, a=1.62717(11) nm, b=0.32788(2) nm, c=0.44200(3) nm, β=104.401(4)º, R_{F2}=0.030). Within the homogeneity range of "Pt_3B", X-ray powder diffraction phase analysis prompted two structure modifications as a function of temperature. The crystal structure of "*h*T-Pt_3B" complies with the hitherto reported structure of anti-MoS_2 (SG $P6_3/mmc$, a=0.279377(2) nm, c=1.04895(1) nm; R_F=0.075, R_I=0.090). The structure of the new "ℓT-Pt_3B" is still unknown. The formation of previously reported $Pt_{\sim 4}B$ has not been confirmed from binary samples. Exploration of the Pt-rich section of Pt-Cu-B system at 600°C revealed a new ternary compound $Pt_{12}CuB_{6-y}$ (X-ray single crystal data: SG $Im\bar{3}$, a=0.75790(2), y=3; R_{F2}=0.0129) which exhibits the filled WAl_{12}-type structure accommodating boron in the interstitial trigonal-prismatic site 12*e*. The isotypic platinum-aluminium-boride was synthesized and studied. Solubility of copper in binary platinum borides has been found to attain about 7 at.% Cu for Pt_2B but to be insignificant for "ℓT-Pt_3B". The architecture of the new Pt_2B structure combines puckered layers of boron filled and empty [Pt_6] octahedra (anti-$CaCl_2$-type fragment) alternating along the *x* axis with a doubled layer of boron-semifilled [Pt_6] trigonal prisms interbedded with a layer of empty tetrahedra and tetragonal pyramids (B-deficient α-TℓI fragment). Assuming boron vacancies ordering (SG *R*3), the $Pt_{12}CuB_{6-y}$ structure exhibits the serpentine-like columns of edge-connected boron filled [Pt_6] trigonal prisms running infinitively along *z* axis and embedding the icosahedrally coordinated Cu atom. Pt_2B, $(Pt_{1-y}Cu_y)_2B$ (y=0.045) and $Pt_{12}CuB_{6-y}$ (y=3) behave metallic, as revealed from temperature dependent electrical resistivity measurements.

INTRODUCTION

In contrast to the plethora of literature on binary transition metal borides, the Pt-B system still remains a puzzle for almost a half of century containing much uncertainties about the composition and crystal structure of phases.

The currently available Pt-B binary phase diagram is based on the investigation from early 1960[thies 1,2] amended by data on the crystal structure of Pt_3B_2 (space group Cmcm, a=0.3371(1) nm, b=0.5817(2) nm, c=0.4045(1) nm)[3]. From a detailed investigation using standard metallographic, thermoanalytic and X-ray diffraction techniques, Wald and Rosenberg[1] found three compounds, i.e. Pt_3B_2 (β phase), Pt_2B (γ phase) and Pt_3B (δ-phase). Two of these borides, Pt_2B and Pt_3B, form by peritectic reactions at 890 °C and 826 °C, respectively, whilst Pt_3B_2 melts congruently at 942 °C and decomposes eutectoidally at 600 °C - 650 °C. DTA data for sintered alloys Pt_3B_2, Pt_2B and Pt_3B, reported by Samsonov and Kosenko (1970)[4] were in accord with the results of Wald and Rosenberg (1965)[1]. Later attempts[5] to shed light on the structural chemistry of phases in the Pt-rich range dealt with the crystal structure of two compounds with tentative compositions $Pt_{\sim 2}B$ and $Pt_{\sim 4}B$; the first one was assigned the anti-MoS_2-type structure (space group $P6_3/mmc$, a = 0.27936 nm, c = 1.0486 nm), whereas the second one was claimed to have a cubic structure with a = 0.75669 nm, however, no atom positions have been reported.

In this contribution we mainly focus on the evaluation of the crystal structures and clarification of the stoichiometry of the phases in the Pt-rich section of the Pt-B phase diagram. The work was initially defined by only two elements, platinum and boron, however during the experiments, we have faced persistent complications due to sluggish phase transformation kinetics which resulted in the formation of multi-phase samples as well as in poor crystallinity and/or ductile alloys. According to numerous studies,[6,7] alloying of platinum with small amounts of transition metals including Cu increases the hardness of platinum alloys and apparently leads to improved crystallinity of ternary platinum based samples. The atomic size difference and electronic and structural relations are favorable for the solubility of Cu in Pt,[8] thus a ternary addition of Cu could well enhance the concentration field of binary platinum based compounds. From the other hand, the transition metal substitution in binary borides in general was reported to affect positively the kinetics of phase transformation and the thermal stability range of binary phases.[9] Subsequently, commencing with the attempt to establish the crystal structures of previously unsolved compounds in the Pt-rich section of Pt-B phase diagram we extended our studies to the ternary Pt-Cu-B system.

In this contribution we (i) present the crystal structure of Pt_2B exhibiting a novel unique binary structure type and (ii) clarify the experimental situation pertinent to the formation and crystal structure of the binary platinum boride, "Pt_3B" (δ-phase). Moreover, we report on synthesis and crystal structure of the first B-filled WAl_{12}-type derivative structure $Pt_{12}CuB_{6-y}$ (y=3) and the isotypic compound with Al as well as provide the information on phase relations in the Pt-Cu-B system at 600 °C within the concentration range relevant to the section of interest in the Pt-B binary boundary. We also present herein temperature dependent electrical resistivity measurements to characterize the new binary and ternary compounds as well as discuss the structural relationships of new structures with already known structure types.

EXPERIMENTAL SECTION

Synthesis and Phase Analysis. Binary and ternary alloys were prepared from ingots of pure elements (Pt foil 99.99 mass %, Ögussa, Austria; crystalline boron 99.8 mass%, ChemPur, Germany; Cu shot 99.999 mass %, ChemPur, Germany; aluminium rod ∅ 6 mm 99.999 mass %, ChemPur, Germany) by repeated arc melting under argon. The arc-melted buttons were cut into pieces, wherefrom one piece was wrapped in tantalum foil and vacuum-sealed in a quartz tube for annealing at different temperatures within 600 – 880 °C for 240 - 1500 hours. The annealed samples were polished applying standard procedures and were examined by scanning electron microscopy (SEM) using a Philips XL30 ESEM with an EDAX XL-30 EDX-detector. X-ray powder diffraction data were collected employing a Guinier-Huber image plate system with monochromatic Cu $K_{\alpha 1}$ radiation ($8^o<2\theta<100^o$) from as-cast and annealed alloys. Alternatively, because significant broadening of diffraction lines was inferred by the powdering process, the powders of alloys were placed in molybdenum containers, sealed in evacuated silica capsules, strain relieved for 30 min at the annealing temperatures and quenched. Quantitative Rietveld refinements of the X-ray powder diffraction data were performed with the FULLPROF program[10] with the use of its internal tables for atom scattering factors.

Differential Scanning Calorimetry. Thermal analyses were performed on a Netzsch 404 Pegasus DSC thermal analyzer under a stream of 6N argon in BN-sprayed Al_2O_3 crucibles. The equipment was calibrated in the temperature range from 300 °C to 1400 °C against pure standard metals supplied by Netzsch to be within ±1 °C. Samples from a set of alloys within the range 66 - 82 at. % Pt: 34 - 18 at.% B annealed at 500 °C for 10 days were heated to the

targeted temperatures at a heating rate of 5 K/min and then cooled to room temperature (5 K/min). These cycles were repeated at least twice to ensure reproducibility. Only the heating curves were used for DTA, as cooling curves show strong supercooling effects particularly within the range $Pt_{66.7}B_{33.3}$ - $Pt_{80}B_{20}$, e.g. $\Delta T/T_m$=0.08 for $Pt_{66.7}B_{33.3}$ and $\Delta T/T_m$=0.13 for $Pt_{68}B_{32}$ where ΔT is the difference between melting temperature (T_m) and crystallization temperature.

Electrical Resistivity. The temperature dependent electrical resistivity of the compounds described above was studied using a four point probe technique and employing a Lakeshore 370 a.c. resistance bridge for temperatures from room temperature down to 0.3 K.

Crystal Structure Determination from X-ray Single Crystal and Powder Diffraction Data. All crystals were isolated via mechanical fragmentation of the annealed samples. X-ray single crystal intensity data were collected on a four-circle Nonius Kappa diffractometer (CCD detector and graphite monochromated Mo Kα radiation) (Pt_2B_{1-x} and $Pt_{12}(Al_{1-x}Pt_x)B_{6-y}$) and a Bruker APEX II diffractometer (CCD detector, κ-geometry, Mo Kα radiation) (for $(Pt_{1-y}Cu_y)_2B$ and $Pt_{12}CuB_{6-y}$); orientation matrices and unit cell parameters were derived with the help of the program DENZO.[11,12] Multi-scan absorption correction was applied using the program SADABS; frame data were reduced to intensity values applying the SAINT-Plus package.[13] The structures were solved by direct methods and refined with the SHELXS-97 and SHELXL-97 programs,[14,15] respectively. Further details concerning the experiments are summarized in Table 1 and Table 2. Detailed descriptions of structural refinements are given below.

Pt_2B_{1-x} and $(Pt_{1-y}Cu_y)_2B$. X-ray diffraction data of Pt_2B_{1-x} single crystal were completely indexed in a monoclinic *C*-centered lattice (*a*=1.62717(11) nm, *b*=0.32788(2) nm, *c*=0.44200(3) nm, *β*=104.401(4)°). The space group *C*2/*m* was indicated by the systematically absent reflections (WinGX program package[16]) and confirmed by the successful structure solution applying direct methods which resulted in three atom positions of platinum (4*i*). Two atom sites of B (4*i* and 2*b*) were found from difference Fourier maps after subsequent refinement of heavy atom positions according to reasonable interatomic distances between detected and proposed atoms. The refinements with free site occupation factors for Pt atoms showed full occupation thus leading to a formula Pt_2B with six formula units per unit cell. The next stages of refinement were carried out inferring anisotropic ADP's for Pt but isotropic for boron atoms and yielded an enlarged value of the displacement parameter for B2 in 2*b* as compared to B1 suggesting a possible fractional population of the B2 atom position. Despite the large differences in scattering factors between boron and platinum do not provide

a reliable refinement of the occupancy parameter for B, there is experimental evidence from X-ray and neutron diffraction data for B vacancies particularly in borides of platinum metals.[2,17,18] Therefore, the variable occupancy of B2 (2*b*) site was tested in further steps of refinements leading to reasonable ADP value at a population level of 93%, thus delivering the formula Pt_2B_{1-x}, x=0.03 for the current crystal ($Pt_{67.3}B_{32.7}$ in at.%) (in further description and analysis denoted as Pt_2B for simplification). The final refinement with fixed occupancy parameter for B2 converged to a reliability factor value of 0.030 exhibiting a residual electron density 4.22 e/Å^3. X-ray powder diffraction intensities collected from the polycrystalline alloys with nominal composition $Pt_{67}B_{33}$ are in best agreement with the intensities calculated from the structural model taken from the single crystal as inferred from Rietveld refinement (Figure 1a).

Unit cell dimensions of single crystal selected from the alloy $Pt_{64}Cu_3B_{33}$ and X-ray powder diffraction spectra recorded from both the annealed and the as-cast samples suggested isotypism with the Pt_2B structure. Analogously direct methods applied to the single crystal data delivered a structure solution with three sites of Pt, one of which, namely 4*i* (*x*,0,*z*), *x*=0.22570(3), *z*=0.2457(1), showed a considerably smaller electron density. Introducing a free variable for the mixed Pt/Cu occupation resulted in 0.865Pt+0.135Cu. The two remaining metal atom sites were found to be occupied by Pt only. Two boron atom positions were readily found in the difference Fourier map. The refinement of the crystal structure proceed with no complication employing anisotropic atom displacement parameters for the metal atom sites, but isotropic temperature factors for the boron atoms. The ADPs of two boron sites in this crystal exhibited a behavior similar to the platinum boride crystal; refinement of B2 occupancy showed an insignificant defect (occ=0.97(7)). The relevant crystallographic data and bond lengths values for the two crystals are given in Table 1.

$Pt_{12}(M_{1-x}Pt_x)B_{6-y}$ (M = Al, Cu). Single crystals have been selected from the samples synthesized in two different ways, (1) arc melted Pt/B buttons (74-76 at.% Pt / 26-24 at.% B) were placed in alumina crucibles, sealed in vacuumed quartz ampoules, heated to slightly above melting temperature (~840 °C) and were slowly (5 deg/h) cooled down to 750 °C; (2) proper amounts of initial elements (Pt, Cu and B) were arc melted, wrapped in Mo foil, vacuum-sealed in a quartz tube and annealed at 600 °C for 240 hours. Scanning electron microscopy of several crystals produced by method (1) revealed the presence of Pt and Al within the ratio range 13:1–9:1, while no additional elements were observed by SEM in the alloy $Pt_{75}Cu_6B_{19}$ synthesized by method (2) showing the metal ratio Pt/Cu=12.

Table 1 X-ray Single Crystal Structure Data[a)] for Pt_2B_{1-x} and $(Pt_{1-y}Cu_y)_2B$

Parameter/Compound	**Pt_2B_{1-x}, x=0.03**	**$(Pt_{1-y}Cu_y)_2B$, y=0.045**
Nominal composition	$Pt_{67.3}B_{32.7}$	$Pt_{63.9}Cu_3B_{33.1}$
Space group; Z	*C*2/*m*, No.12; 6	
Structure type	**Pt_2B**	
Formula from refinement	$Pt_2B_{0.97}$	$Pt_{1.91}Cu_{0.09}B_{0.99}$
Diffractometer	Nonius Kappa	Bruker APEX II
Range for data collection	2.58<θ <30.00	2.58<θ <33.20
Crystal size	35x40x25 μm^3	35x35x30 μm^3
a [nm]	1.62717(11)	1.6267(3)
b [nm]	0.32788(2)	0.32698(6)
c [nm]	0.44200(3)	0.43855(8)
β [deg]	104.401(4)	104.316(5)
Reflections in refinement	333 $F_o > 4\sigma(F_o)$ of 365	424 $F_o > 4\sigma(F_o)$ of 483
Mosaicity	<0.4	<0.4
Number of variables	24	26
$R_F^2 = \Sigma\|F_0^2-F_c^2\|/\Sigma F_0^2$	0.030	0.026
R_{Int}	0.034	0.0576
GOF	1.073	1.042
Extinction (Zachariasen)	0.0020(2)	0.0006(1)
M1 in 4*i* (*x*, 0, *z*); occ.; U_{11}[b], U_{22}, U_{33}, $U_{23}=U_{12}=0$, U_{13}	*x*=0.05365(4), *z*=0.3011(1); 1.00 Pt1; 0.0029(4), 0.0098(4), 0.0032(3), -0.0002(3)	*x*=0.05454(3), *z*=0.3015(1); 1.00 Pt1; 0.0071(3), 0.0095(2), 0.0061(2), -0.0000(2)
M2 in 4*i* (*x*, 0, *z*); occ.; U_{11}, U_{22}, U_{33}, $U_{23}=U_{12}=0$, U_{13}	*x*=0.22523(4), *z*=0.2443(1); 1.00 Pt2; 0.0015(4), 0.0072(4), 0.0029(4), -0.0004(3)	*x*=0.22570(3), *z*=0.2457(1); 0.865(3)Pt2+0.135(3)Cu22; 0.0060(3), 0.0089(3), 0.0079(3), 0.0006(2)
M3 in 4*i* (*x*, 0, *z*); occ.; U_{11}, U_{22}, U_{33}, $U_{23}=U_{12}=0$, U_{13}	*x*=0.38874(4), *z*=0.1682(1); 1.00 Pt3; 0.0021(4), 0.0062(3), 0.0034(3), -0.0001(3)	*x*=0.38810(3), *z*=0.1670(1); 1.00Pt3; 0.0064(2), 0.0065(2), 0.0075(2), 0.0002(2)
B1 in 4*i* (*x*, 0, *z*); occ.; U_{iso}[c]	*x*=0.177(1), *z*=0.653(4); 1.00; 0.010(3)	*x*=0.176(1), *z*=0.658(3); 1.00; 0.008(2)
B2 in 2*b* (0, ½, 0); occ.; U_{iso}	0.93(7); 0.014(5)	0.97(7); 0.013(4)
Residual density; max; min [electrons/nm^3]x1000	4.22; -4.90	4.49; -3.42

Interatomic distances (nm)

Pt_2B_{1-x}, x=0.03		**$(Pt_{1-y}Cu_y)_2B$, y=0.045**	
Pt1 - 2 B2 0.2155(1)	Pt3 - B2 0.2121(1)	Pt1 - 2 B2 0.2151(1)	Pt3 - B2 0.2123(1)
Pt1 - B1 0.221(2)	Pt3 - 2 B1 0.221(1)	Pt1 - B1 0.220(1)	Pt3 - 2 B1 0.218(1)
Pt1 - Pt1 0.2769(1)	Pt3 - Pt2 0.27636(7)	Pt1 - Pt1 0.2776(1)	Pt3 - M2 0.27475(9)
Pt1 - Pt1 0.2797(1)	Pt3 - 2 Pt2 0.27871(7)	Pt1 - Pt1 0.2797(1)	Pt3 - 2 M2 0.27782(6)
Pt1 – 2 Pt3 0.28242(6)	Pt3 - 2 Pt1 0.28242(6)	Pt1 – 2 Pt3 0.28109(6)	Pt3 - 2 Pt1 0.28109(6)
Pt1 - Pt2 0.28647(7)	Pt3 - 2 Pt1 0.29724(6)	Pt1 - M2[d] 0.28547(9)	Pt3 - 2 Pt1 0.29517(6)
Pt1 - 2 Pt3 0.29724(6)	Pt3 - 2 Pt1 0.30739(8)	Pt1 - 2 Pt3 0.29517(6)	Pt3 - 2 Pt1 0.30922(8)
Pt1 - 2 Pt3 0.30739(8)	Pt3 - 2 Pt3 0.32788(2)	Pt1 - 2 Pt3 0.30920(8)	Pt3 - 2 Pt3 0.32698(6)
Pt1 - 2 Pt1 0.32788(2)		Pt1 - 2 Pt1 0.32698(6)	
	B1 - Pt2 0.214(2)		B1 - M2 0.215(1)
Pt2 - B1 0.214(2)	B1 - 2 Pt3 0.221(1)	M2 - B1 0.215(1)	B1 - 2 Pt3 0.218(1)
Pt2 - 2 B1 0.225(1)	B1 - Pt1 0.221(2)	M2 - 2 B1 0.225(1)	B1 - Pt1 0.220(1)
Pt2 - B1 0.253(2)	B1 - 2 Pt2 0.225(1)	M2 - B1 0.250(1)	B1 - 2 M2 0.225(1)
Pt2 - 2 Pt2 0.27463(8)	B1 - Pt2 0.253(2)	M2 - 2 M2 0.27205(9)	B1 - M2 0.250(1)
Pt2 - Pt3 0.27636(7)		M2 - Pt3 0.27475(9)	
Pt2 - 2 Pt3 0.27871(7)	B2 - 2 Pt3 0.2121(1)	M2 - 2 Pt3 0.27782(6)	B2 - 2 Pt3 0.2123(1)
Pt2 - Pt1 0.28647(7)	B2 - 4 Pt1 0.2155(1)	M2 - Pt1 0.28547(9)	B2 - 4 Pt1 0.2151(1)
Pt2 - 2 Pt2 0.29775(8)		M2 - 2 M2 0.29638(8)	
Pt2 - 2 Pt2 0.32788(2)		M2 - 2 M2 0.32698(6)	

[a] crystal structure data are standardized using the program Structure Tidy[19], [b, c] anisotropic (U_{ij}) and isotropic (U_{iso}) atomic displacement parameters are given in [10^2 nm^2], [d] M2=0.865(3)Pt2+0.135(3)Cu22

Analyses of the X-ray data set collected from the Al containing single crystal, particularly the systematic extinctions (observed for $h+k+l$=2n+1, 0kl for $k+l$=2n+1, hhl for l=2n+1 and 00l for l=2n+1), prompted a body-centered cubic unit cell (a=0.75790(2) nm) consistent with space group symmetries *Im*-3 (no. 204), $I2_13$ (no. 199) and *I*23 (no. 197), out of which the highest symmetric one, *Im*-3, was chosen for further structure analysis. Direct methods delivered a structure solution with two sites for metal atoms: one site (24*g*) consistent with a full occupation by Pt atoms and a 2*a* site with a considerably smaller electron density. Introducing a free variable for the mixed Al/Pt occupation of the 2*a* site resulted in 0.893(3) Al+0.107(3) Pt. The B atom is easily found on the 12*e* site (x,0,1/2; x=0.1125), however, the low value of residual electron density of only 4.04 e–/Å^3 hinted towards a fractional population which was further refined to about 58% B. The large difference in the scattering power between platinum and boron imposes difficulties in defining the positional parameter at the low boron population level, therefore the positional and occupancy parameters as well as ADP for boron in this structure were alternately constrained to a pre-refined value at each consequent cycle of refinement until reaching convergence with anisotropic ADP's for Pt and Pt/Al at a reliability factor value as low as R_F=0.0169.

The single crystal of $Pt_{12}CuB_{6-y}$ showed practically identical behaviour with respect to the boron atom parameters. Refinement of mixed occupancy on the individual metal atom positions revealed no disorder leading to fully occupied Pt and Cu atom sites (24*g* and 2*a* respectively) at a 50% population of the B site.

We should note that in both crystals, in the case of dismissing positional parameter constraints of B, the atom is drifting along x until reaching the vicinity of a symmetry equivalent boron (x=0.092(8), d_{B-B}=0.14(1) nm for $Pt_{12}CuB_{6-y}$ and x=0.087(5), d_{B-B}=0.132(8) nm for $Pt_{12}(Al_{1-x}Pt_x)B_{6-y}$). The short distance between boron atoms excludes their simultaneous presence; besides, the partial occupancy of boron atom position supports the understanding that only an average structure has been determined. The results of the refinements are summarized in Table 2.

Boron vacancies ordering could be achieved in the space group *R*3 (*Im*-3 (no. 204) → *t*2 → *I*23 (no. 197); $a_1=a_0$, $b_1=b_0$, $c_1=c_0$; *I*23 (no. 197) → *t*4 → R3 (no. 146) $a_2=-b_1+c_1$, $b_2=a_1-c_1$, $c_2=½a_1+½b_1+½c_1$). Assuming the pseudo-cubic lattice but trigonal symmetry, e.g. for $Pt_{12}CuB_{6-y}$ crystal (a=1.0678 nm, c=0.6539 nm, $\alpha=\beta$=90º, γ=120º), the *hkl* data were transformed to trigonal setting; consequent refinement in *R*3 revealed the split of 12*e* B atom position of the parent high-symmetry space group in two symmetry independent Wyckoff sites 9*b* (x,y,z) of which only one (x=0.026(2), y=0.467(2), z=0.058(4), B_{iso}=0.014(5)) was

completely occupied by boron. Despite this possibility, careful inspection of the intensity frames did not reveal any hints for symmetry reduction. Moreover, X-ray powder diffraction intensities collected from the polycrystalline alloy with nominal composition $Pt_{74}Cu_7B_{19}$ were in good agreement with the intensities calculated from the cubic structural model obtained from the single crystal as inferred from Rietveld refinement (Figure S1 in Supporting Information). Hence the choice of space group has been confined to higher symmetric *Im*-3 and further structure analysis will be performed according to the results of refinement in this space group.

Table 2. X-ray Single Crystal Structure Data[a)] for $Pt_{12}(Pt_{1-x}Al_x)B_{6-y}$ and $Pt_{12}CuB_{6-y}$

Parameter/Compound	**$Pt_{12}(Al_{1-x}Pt_x)B_{6-y}$, x=0.107, y=2.5**	**$Pt_{12}CuB_{6-y}$, y=3**
Nominal composition	$Pt_{73.4}Al_{5.4}B_{21.2}$	$Pt_{75}Cu_{6.3}B_{18.7}$
Space group	*Im* $\bar{3}$; No. 204	
Structure type	$Pt_{12}CuB_{6-y}$ (filled WAl_{12}-type)	
Formula from refinement	$Pt_{12.107}Al_{0.893}B_{3.5}$	$Pt_{12}CuB_3$
Range for data collection	7.62°<θ<34.78°	5.40°<θ<29.58°
Diffractometer	Nonius Kappa	Bruker APEX II
Crystal size	35x35x35μm^3	40x40x40 μm^3
a [nm], single crystal XRD data *a* [nm], powder XRD data	0.75790(2) 0.75878(2)	0.75506(2) 0.75529(2)
Reflections in refinement	176 F_o >4σ(F_o) of 186	110 F_o >4σ(F_o) of 124
Mosaicity	<0.4	<0.4
Number of variables	12	12
$R_F^2 = \Sigma\|F_0^2-F_c^2\|/\Sigma F_0^2$	0.0169	0.0129
R_{Int}		
GOF	1.133	1.130
Extinction (Zachariasen)	0.00098(7)	0.00015(3)
M1 in 2*a* (0, 0, 0); occ.; U_{11}[b]=U_{22}=U_{33}, U_{23}=U_{13}=U_{12}=0	0.893(4) Al1 + 0.107(4) Pt11; 0.020(1);	1.00 Cu1; 0.0064(8)
M2 in 24*g* (0, *y*, *z*); occ.; U_{11}, U_{22}, U_{33}, U_{23}, U_{13}=U_{12}=0	*y*=0.18638(4), *z*=0.30503(4); 1.00 Pt1; 0.0080(2), 0.0090(2), 0.0094(2), -0.0000(1)	*y*=0.18542(5), *z*=0.30671(5); 1.00 Pt1; 0.0067(2); 0.0070(2); 0.0064(2); -0.0004(1)
B1 in 12*e* (*x*, 0, ½); occ.; U_{iso}[c]	*x*=0.1125[d]; 0.58(5); 0.047(7)	*x*=0.1123[d]; 0.50(5); 0.04(1)
Residual density; max; min [electrons/nm^3]x1000	4.25; -2.54	1.456; -1.891

Interatomic distances (nm)

$Pt_{12}(Al_{1-x}Pt_x)B_{6-y}$, x=0.107, y=2.5				**$Pt_{12}CuB_{6-y}$, y=3**			
Pt1 – B1	0.21227(3)	M1 – 12 Pt1	0.27092(3)	Pt1 – B1	0.21127(5)	Cu1 – 12 Pt1	0.27061(6)
Pt1 - 2 B1	0.22150(3)			Pt1 - 2 B1	0.21929(5)		
Pt1 - M1[e]	0.27092(3)	B1 – 2 Pt1	0.21227(3)	Pt1 - Cu1	0.27061(6)	B1 – 2 Pt1	0.21127(5)
Pt1 – 4 Pt1	0.27996(3)	B1 - 4 Pt2	0.22150(3)	Pt1 – 4 Pt1	0.27885(6)	B1 - 4 Pt2	0.21929(5)
Pt1 – Pt1	0.28251(5)			Pt1 – Pt1	0.28001(9)		
Pt1 - 4 Pt1	0.28546(3)			Pt1 - 4 Pt1	0.28569(6)		
Pt1 - Pt1	0.29554(4)			Pt1 - Pt1	0.29189(7)		

[a] crystal structure data are standardized using the program Structure Tidy[19], [b, c] anisotropic (U_{ij}) and isotropic (U_{iso}) atomic displacement parameters are given in [10^2 nm^2], [d] fixed parameter, [e] M1= 0.893(4) Al1 + 0.107(4) Pt11

CIF data have been deposited with Fachinformationszentrum Karlsruhe, 76344 Eggenstein-Leopoldshafen, Germany [fax: (49) 7247-808-666; e-mail: crysdata@fiz-karlsruhe.de] with

depository numbers CSD-430130 for Pt_2B_{1-x}, CSD-430131 for $(Pt_{1-y}Cu_y)_2B$, CSD-430132 for $Pt_{12}CuB_{6-y}$ and CSD-430133 for $Pt_{12}(Pt_{1-x}Al_x)B_{6-y}$.

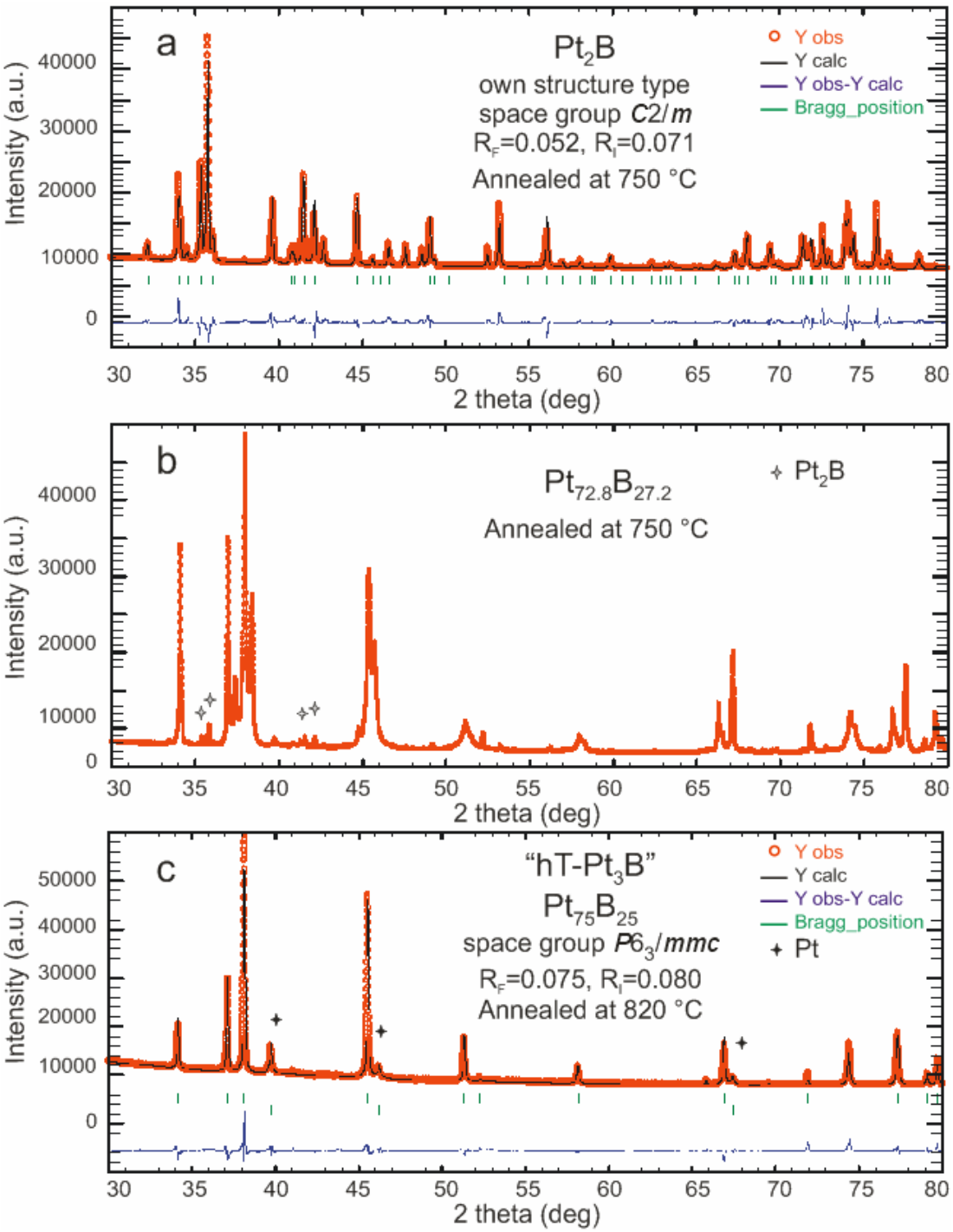

Figure 1. X-ray diffraction patterns of Pt_2B (a) and "hT-Pt_3B" (c) in comparison with "ℓT-Pt_3B" (b). The solid line derives from Rietveld refinement. $Y_{obs.}$-$Y_{calc.}$ is the intensity difference between exprimental data and Rietveld calculations.

RESULTS AND DISCUSSION

Pt_2B and $(Pt_{1-y}Cu_y)_2B$: Structural Description and Analysis. The Pt_2B compound represents a new binary structure type of borides. There are three and two independent atom sites of platinum and boron in the unit cell respectively of which solely the Pt2 atom site is prone to Pt/Cu substitution. Thus, $(Pt_{1-y}Cu_y)_2B$ is part of a solid solution of Cu in binary Pt_2B. B2 is octahedrally coordinated exclusively by Pt atoms both in pure and copper substituted diplatinum boride, while the metal coordination around the atom B1 for $(Pt_{1-y}Cu_y)_2B$ is a trigonal prism formed by three Pt and three atoms M2=0.865(3)Pt2+0.135(3)Cu22 (in further description denoted as M2) (Figure 2a). One rectangular face of the trigonal prism around B1 is capped by either Pt or M2. Coordination polyhedra around metal atoms all exhibit 14 vertices, among which 3, 4, and 3 apices are occupied by boron for Pt1, Pt2 (or M2) and Pt3, respectively (Table 1 and Figure 2f-h).

The unit cell exhibits the packing of two slabs interleaving infinitively along the *x* axis (Figure 2a). One slab (A) represents a puckered layer (in *bc* plane), which is composed of columns of B-filled octahedra formed by six Pt atoms and columns of empty [Pt_6] octahedra (denotes a vacancy in 2*d* (0, ½, ½) with d_{-Pt} = 0.203-0.215 nm). Those columns run along the *b* direction and interchange with each other along *c*. The octahedra within the columns are inter-linked via common edges leaving empty a little space in a shape of tetrahedra [Pt_4], while the empty and B-filled octahedra from different columns fuse via common faces thus leading to a corrugation of the layer in the *bc* plane. Such arrangement of B-filled and empty octahedra has been observed also in the Pd_2B structure[20] (Figure 2b) which forms the anti-$CaCl_2$-type[21]. It should be emphasized that the residual electron density reveals no hint for an additional foreign atom in the 2*d* Wyckoff site.

Block B (Figure 2a) is composed of B-filled and empty trigonal prisms formed by all three kinds of metal atoms, Pt1, Pt3 and Pt2 (or M2); the prisms interlink via common rectangular faces to form rows running infinitively along the *b* direction. The width of block B along *a* is confined to two trigonal prisms sharing common triangular faces. The condensation of slabs formed by B-filled and empty trigonal prisms in the *c* direction follows the pattern observed in the CrB structure[22] (α-TlI-type[23]) (Figure 2c), which exhibits the intergrowth of AlB_2-type slabs (sheets of B-centered trigonal prisms) and W-type slabs (empty tetrahedra and tetragonal pyramids).[19] However, while in CrB every trigonal prism in

the row is centered by a boron atom, which forms infinite zigzag -B-B- chains, every sequent prism is empty in the Pt_2B structure (Figure 2e) thus delivering the fragment of the WC-type[24] (a vacant variant of AlB_2) (Figure 2d).

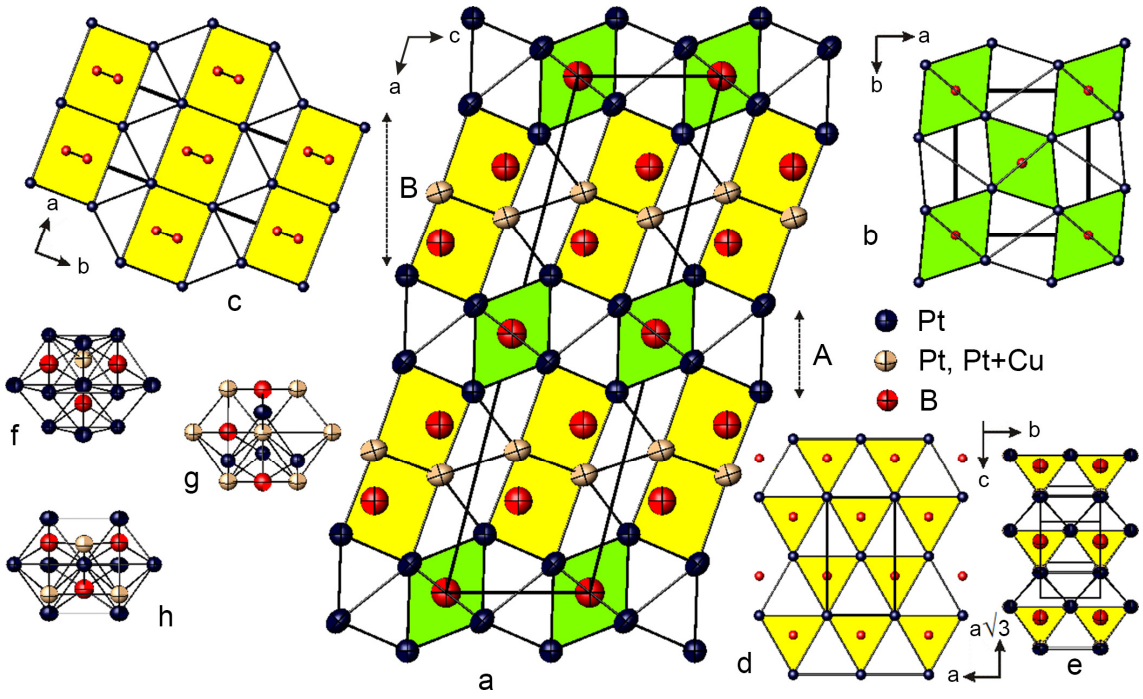

Figure 2. Pt_2B-type structure of $(Pt_{1-y}Cu_y)_2B$ (a) as arrangement of Pd_2B (slab A, anti-$CaCl_2$-type) (b) and B-deficient CrB (slab B, α-TlI-type) units (c). Nearest-neighbouring atom environments of boron are emphasized: [B1$Pt2_3$ (or M_3)$Pt1_1Pt3_2$] trigonal prisms – yellow, [B2$Pt3_2Pt1_4$] octahedra – green. Empty polyhedra are left open. A ½ B slab ($0.05<x<0.23$) of Pt_2B (and $(Pt_{1-y}Cu_y)_2B$) (e) in comparison with the WC-type (d). Coordination polyhedra [Pt1$B_3Pt_{10}Pt2_1$ (or $M)_1$], [Pt2(or M)B_4Pt2_6(or M_6)Pt_4] and [Pt3B_3Pt2_3(or M_3)Pt_8] (f, g and h respectively). The atoms for the Pt_2B-type are represented by their thermal ellipsoids.

$Pt_{12}(Al_{1-x}Pt_x)B_{6-y}$ and $Pt_{12}CuB_{6-y}$: Structural Description and Analysis. Structure analysis from powder X-ray diffraction data showed that the title compounds form B-filled variants of the WAl_{12}-type[25] (space group *Im*-3, a=0.75803 nm, Al in 24 *g*: 0,*y*,*z*, *y*=0.184, *z*=0.309; W in 2*a*: 0,0,0). In WAl_{12}, tungsten is surrounded by twelve Al atoms. Each aluminium atom has one W and ten Al neighbours. WAl_{12} exhibits rather large octahedral and trigonal prismatic voids centered at 8*c* (¼,¼,¼) and 12*e* (*x*,0,½), respectively (Figure 3a). Each two trigonal prisms are coupled by common rectangular faces and linked with another double prism assembly by a common edge in such a way that the prism axes are perpendicular. In the

ternary platinum borides $Pt_{12}(Al_{1-x}Pt_x)B_{6-y}$ and $Pt_{12}CuB_{6-y}$ boron atoms randomly reside in the trigonal prismatic 12*e* site of the $Pt_{12}M$ (M=Al/Pt, Cu) framework, while the octahedral voids remain vacant. Assuming partial occupancy of the 12*e* site by B, only one of the prisms coupled by rectangular faces is inhabited (Figure 3c). The structure can be more conveniently visualized in rhombohedral setting: serpentine-like columns of edge connected trigonal prisms $[BPt_6]$ run infinitively along the *c* direction (Figure 3e). The coordination polyhedron of M1 is an icosahedron $[MPt_{12}]$ (Figure 3d). Pt1 is coordinated by 14 atoms, $[Pt1B_3CuPt_{10}]$ (Figure 3b).

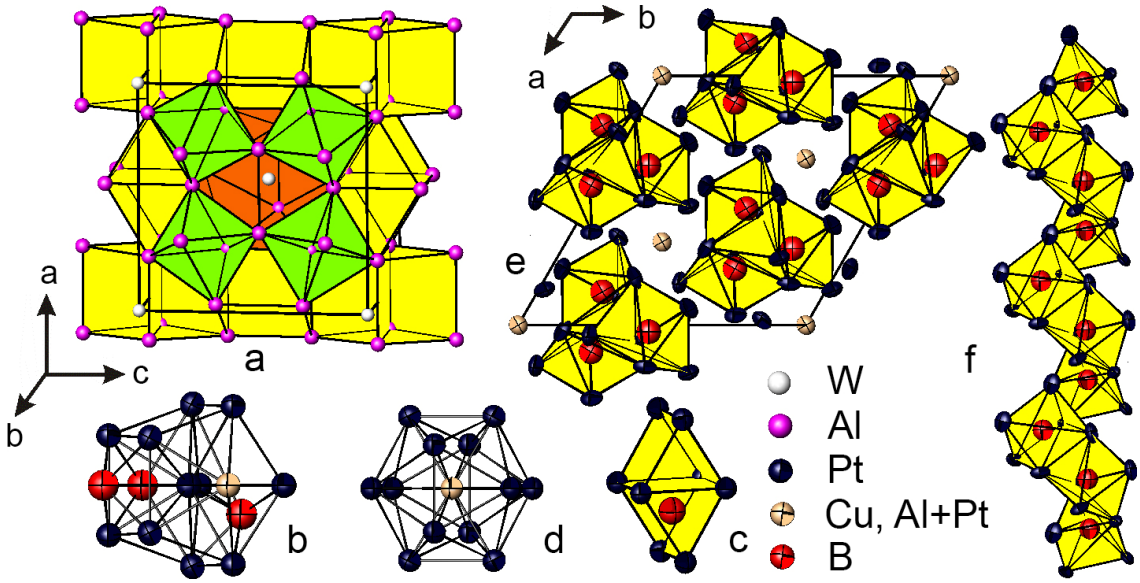

Figure 3. Crystal structure of WAl_{12} exhibiting a framework of vacant [Al6] trigonal prisms (yellow) and [Al6] octahedra (green) enveloping the W atom (a). Coordination polyhedra of atoms in the average B-filled WAl_{12}-type structure: Pt1 (b), face-coupled $[Pt_6]$ trigonal prisms in the case that only one of them is boron populated (c), and M=Cu, Al+Pt (d). Representation of $Pt_{12}(Al_{1-x}Pt_x)B_{6-y}$ and $Pt_{12}CuB_{6-y}$ structures in rhombohedral setting (e) illustrating columns of edge connected boron filled $[BPt_6]$ trigonal prisms (f) running along *c* direction.

The B-filled WAl_{12}-type structure has never been observed hitherto for ternary borides. Hassler et al. (1979)[5] reported on the existence of a binary $Pt_{\sim 4}B$ compound, a=0.75669(5) nm claiming structural features similar to $Pt_{12}(Al_{1-x}Pt_x)B_{6-y}$ and $Pt_{12}CuB_{6-y}$. A related structure with vacant trigonal prismatic voids, but populated octahedral voids is adopted by the large family of skutterudites, $LaFe_4Sb_{12}$.[26] Platinum substructures in $Pt_{12}(Al_{1-x}Pt_x)B_{6-y}$ and $Pt_{12}CuB_{6-y}$ are similar to that observed for the rare earth atoms in Ho_6Co_2Ga[27] and its

disordered derivative $Ho_{12}Co_5Bi$[28]. Trigonal prismatic voids of the WAl_{12}-type arrangement accommodating transition metal atoms have been reported for the large families of rare earth transition metal indides and plumbides $RE_{12}Pb(In)Ni(Co)_6$ (space group *Im*-3; Ni (or Co) in 2*a*);[29] similarly to the platinum boride structures, the transition metal atoms exhibit short distances to the symmetry equivalent atom as compared with the sum of atom radii at full occupancy of the atom site.

Binary Pt-B System and Pt-rich Region of the Pt-Cu-B Ternary System from DTA and X-ray Powder Diffraction Data. The invariant temperatures from DTA recorded for the samples within the compositions $Pt_{65}B_{34}$ – $Pt_{75}B_{25}$ are slightly higher than those reported by Wald and Rosenberg (1965),[1] however, inconsistency arises between the hitherto presented crystallographic data on $Pt_{\sim 4}B$ and $Pt_{\sim 2}B$[5] and the structural features derived in this work for the platinum rich binary borides.

DTA investigations into Pt-B system in the region 65 at.%- 80 at.% Pt. The evaluation of DTA heating runs (tangent method) on several as cast and annealed alloys essentially confirmed the phase relations reported by Wald and Rosenberg (1965),[1,30] although the isothermal reactions in our analyses appear at slightly higher temperatures: peritectic formation of Pt_3B: L+(Pt)↔Pt_3B at 831±8 °C, eutectic reaction: L↔Pt_3B+Pt_2B at 794±8 °C and peritectic formation of Pt_2B: L+Pt_3B_2↔Pt_2B at 900±10 °C. In none of the recordings (heating at 5 K/min as well as rapid quenching at 80 K/min) a trace of a phase transition could be seen in the temperature region scanned (200 to 950°C), although independent isothermal heating experiments for Pt_3B revealed a change in the XRD spectrum at around 800 °C (see above). This fact indicates a rather low heat content and/or sluggish reaction kinetics for the solid-solid phase transition "hT-Pt_3B"↔"ℓT-Pt_3B".

Pt-B phase diagram from X-ray powder diffraction studies. According to altering of lattice parameters of single phase and multiphase samples within 65 at.%-68 at.% Pt, Pt_2B has a small homogeneity range, which decreases above 600 °C as deduced from lattice parameters variations (*a*=1.62430(3) nm, *b*=0.32728(1) nm, *c*=0.44223(1) nm, *β*=104.405º at 600 °C and *a*=1.62448(4) nm, *b*=0.32724(1) nm, *c*=0.44274(1) nm, *β*=104.421(1)º at 880 °C; Rietveld refinement of X-ray powder diffraction patterns) and from alteration of the unit cell volume with temperature: 0.22770(1) nm^3 (B-rich end) - 0.22792(1) nm^3 (B-poor end) at 600 °C to 0.22802(1) nm^3 (B-rich end) - 0.22804(1) nm^3 (B-poor end) at 750 °C and to 0.22800(1) nm^3 at 880 °C. The concentration range 72 at.% - 75 at.% Pt is characterized by the formation of

"Pt_3B" in good agreement with the report on the constitution of the Pt-B phase diagram by Wald and Rosenberg (1965) (δ-phase).[1] The analysis of the X-ray powder diffraction spectra for the $Pt_{73}B_{27}$ - $Pt_{75}B_{25}$ samples annealed within 600 °C - 820 °C revealed the existence of two structural forms for the "Pt_3B", high temperature ("hT-Pt_3B") and low temperature ("ℓT-Pt_3B") structures above and below appr. 800(±5) °C, respectively. The X-ray powder diffraction pattern of "hT-Pt_3B" could be indexed with a hexagonal unit cell, a=0.279346(5) nm, c=1.04894(3) nm and a=0.279231(4) nm, c=1.04867(2) nm for the boron rich and boron-poor ends, respectively. The existence of a boride with the hexagonal structure of anti-MoS_2-type has been proposed by Hassler et al. (1979).[5] However, rather high values of reliability factors ($R_F=\Sigma|F_o-F_c|/\Sigma F_o=0.075$ and $R_I=\Sigma|I_o-I_c|/\Sigma I_o=0.090$ for space group $P6_3/mmc$ [(no. 194), a=0.279377(2) nm, c=1.04895(1) nm, Pt in 4*f* (⅓,⅔,*z*; *z*=0.61370(6), occ. 1.0 (fixed)) and B in 2*c* (⅓,⅔,¼; occ. 0.65 (fixed))] obtained from Rietveld refinement of X-ray powder diffraction intensity data of the high temperature phase applying the MoS_2 structure model (Figure 1c) do not provide satisfactory evidence for a correct assignment of the structure type. The X-ray powder pattern of the low temperature phase is still unknown (Figure 1b); numerous selected crystals of both "hT-Pt_3B" and "ℓT-Pt_3B" showed insufficient quality for further studies.

The formation of a binary compound $Pt_{\sim 4}B$ with a cubic structure (*cI*, a=0.75669 nm) claimed by Hassler et al. (1979)[5] has not been confirmed in the current work, however, the $Pt_{74}B_{26}$-$Pt_{75}B_{25}$ samples, which were melted in Al_2O_3 crucibles at ~840 °C, randomly exhibited the formation of crystalline portions obviously formed due to attack of the crucibles. The single crystal X-ray diffraction study for one of the specimens, $Pt_{12}(Pt_{1-x}Al_x)B_{6-y}$, is given in the preceding section along with the structural study of $Pt_{12}CuB_{6-y}$.

Solubility of boron in platinum is rather small as inferred from the lattice parameter variation of Pt(B) in alloys within the binary equilibrium field (Pt) + "Pt_3B" ($a_{Pt(B)}$=0.39233(1) nm at 600 °C and $a_{Pt(B)}$=0.39249(1) nm at 820 °C) in comparison with the lattice parameter of pure Pt (a_{Pt}=0.39227 nm,[30] a_{Pt}=0.3922 nm at 850 °C[31]).

Phase relations in the Pt-rich corner of the ternary system Pt-Cu-B at 600 °C. The following paragraph briefly describes the results of our experiments focused on ternary phase equilibria at 600 °C relevant to the Pt_2B - "Pt_3B" section of the binary system (≥60 at.% Pt). The formation and crystal structures of binary borides described above have been confirmed from ternary Pt-Cu-B samples. The copper solubility in Pt_2B is about 7 at.% as inferred from SEM and X-ray powder diffraction phase analyses (a=1.62327(2) nm, b=0.32639(1) nm,

c=0.43845(1) nm, β=104.373(1)° for $(Pt_{1-y}Cu_y)_2B$, y=0.1). "ℓT-Pt_3B" does not dissolve a significant amount of copper. The main feature is the presence of the ternary phase $(Pt_{12-x}Cu_x)CuB_{6-y}$ ($0 \le x \le 1.6$, *a*=0.7558 nm - 0.7524 nm and *a*=0.7565 nm - 0.7531 nm for boron poor and boron rich ternary samples, respectively) existing in equilibrium with Pt(Cu),[32,33] "ℓT-Pt_3B" and $(Pt_{1-x}Cu_x)_2B$ as well as with a new ternary compound ~$Pt_{60}Cu_{15}B_{25}$ exhibiting an unknown structure.

Electrical Resistivity of Pt_2B, $(Pt_{1-y}Cu_y)_2B$ (y=0.045) and $Pt_{12}CuB_{6-y}$ (y=3). The temperature dependent electrical resistivity of the compounds listed above has been studied using a 4-point method in a range from room temperature down to 0.3 K. Pt_2B exhibits a metallic-like behavior without any phase transitions in the entire temperature range studied. A least-square fit (solid line, Figure 4a) of the Bloch-Grüneisen-Mott[34] model,

$$\rho_{B-G-M} = \rho_0 + C\frac{T^5}{\theta_D{}^6}\int_0^{\theta_D/T}\frac{x^5}{(e^x-1)(1-e^{-x})}dx - AT^3, \qquad (1)$$

was applied to the experimental data, deriving the Debye temperature $\theta_D = 177$ K, the residual resistivity $\rho_0 = 7.46\,\mu\Omega cm$ and a Mott coefficient $A = 2.7*10^{-11}\,\mu\Omega cm/K^3$. The so-called Mott–Jones term, AT^3, has to be added to account for corrections due to scattering of conduction electrons on a narrow *d*-band in the vicinity of the Fermi energy. The relatively low residual resistivity refers to a fairly good sample quality and the absence of a substantial number of predominantly B vacancies.

The electrical resistivity of $(Pt_{1-y}Cu_y)_2B$ (y=0.045) in addition to its metallic behavior, evidences a noticeable curvature in the temperature region around 100 K. The experimental curve has been analyzed using the model described above, delivering $\theta_D = 124$ K, $\rho_0 = 29.9\,\mu\Omega cm$ and $A = 5.8*10^{-8}\,\mu\Omega cm/K^3$. The reduced value of the residual resistivity ratio RRR ~2 points to an increased disorder in the sample, due to the inclusion of copper in the solid solution.

The temperature dependent electrical resistivity of $Pt_{12}CuB_{6-y}$ (Figure 4b), on the other hand, exhibits a much stronger curvature than the previous systems and, additionally, a tendency towards saturation in the high temperature region making an analysis, using Eqn. 1, impossible. Instead, the parallel resistance model[35] is considered, i.e.,

$$\frac{1}{\rho} = \frac{1}{\rho_{B-G}} + \frac{1}{\rho_{sat}}, \qquad (2)$$

where ρ_{B-G} corresponds to the Bloch-Grüneisen model and ρ_{sat} is the resistivity in the high temperature limit. As the result of a least squares fit $\theta_D = 155\ \mathrm{K}$, $\rho_0^* = 215\,\mu\Omega cm$ and $\rho_{sat} = 149\,\mu\Omega cm$ were acquired. The much larger overall resistivity of $Pt_{12}CuB_3$, compared to the remaining ones, obviously refers to B vacancies, which turn out to be very efficient scattering centers.

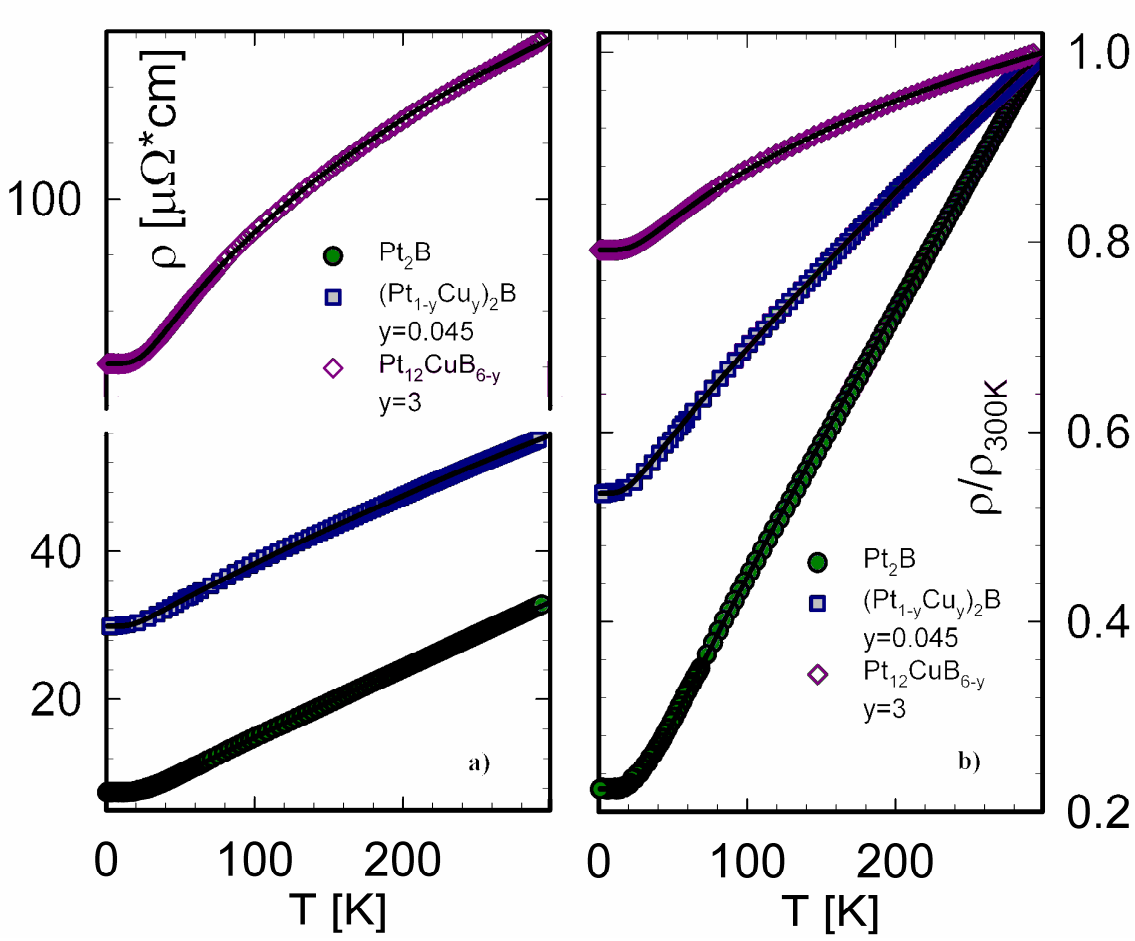

Figure 4. Temperature dependent electrical resistivity of Pt_2B, $(Pt_{1-y}Cu_y)_2B$ (y=0.045) and $Pt_{12}CuB_{6-y}$ (y=3) compounds (a) and presented as ρ / ρ_{300K} (b). Solid lines correspond to least squares fits of models described in text.

CONCLUSIONS

The Pt-rich parts of Pt-B and Pt-Cu-B systems have been investigated with respect to formation and crystal structure of compounds. Pt_2B crystallizes in its own structure type and exhibits an arrangement of anti-$CaCl_2$-type and B-deficient TℓI-type fragments interleaving infinitely along the *a* axis. Consequently, two types of coordination figures are inherent for boron atoms: a metal octahedron and a trigonal prism. Pt_2B forms peritectically at 900±10 °C by the reaction $L+Pt_3B_2 \leftrightarrow Pt_2B$ and exists within a narrow concentration field as detected from lattice parameters variations. Two phases were found to exist within the "Pt_3B" compositional range. The X-ray powder diffraction pattern of the high temperature phase existing above 800 °C tentatively agrees with the previously reported anti-MoS_2-type structure, however, Rietveld refinement converged to fairly poor values of reliability factors of R_F=0.075 and R_I=0.090 at 65% occupancy of the boron atom position thus implying further structural studies. The low temperature phase forms an unknown structure. Whilst binary Pt_2B extends into the ternary Pt-Cu-B region with a solubility range limited at 600 °C to 7 at.% Cu, the solubility of Cu in low-temperature "ℓT-Pt_3B" is negligible. Investigation of the Pt-Cu-B system at 600 °C in the Pt-rich corner resulted as well in the discovery of a new ternary phase $(Pt_{12-x}Cu_x)CuB_{6-y}$ ($0 \le x \le 1.6$, y=3), which according to X-ray single crystal intensity data constitutes the first B-filled version of the WAl_{12}-type. The platinum-aluminium-boride system forms an isotypic compound, $Pt_{12}(Al_{1-x}Pt_x)B_{6-y}$. In both structures ($(Pt_{12-x}Cu_x)CuB_{6-y}$ and $Pt_{12}(Al_{1-x}Pt_x)B_{6-y}$) boron atoms are found exclusively in [Pt_6] trigonal prisms; in case of boron vacancies ordering, the B-filled trigonal prisms interconnect via common edges to form serpentine-like columns running infinitely along the *c* axis. The existence of previously reported binary "$Pt_{\sim 4}B$" compound has not been confirmed neither from binary nor from ternary samples.

Pt_2B, $(Pt_{1-y}Cu_y)_2B$ (y=0.045) and $Pt_{12}CuB_{6-y}$ (y=3) exhibit a metallic type of conductivity as inferred from temperature dependent electrical resistivity measurements.

ASSOTIATED CONTENT

Supporting Information

X-ray crystallographic data in CIF format; Rietveld refinement of X-ray powder diffraction intensity data of $Pt_{12}CuB_{6-y}$ (y=3).

AUTHOR INFORMATION

Corresponding Author

**E-mail address: oksana.sologub@univie.ac.at*

Notes

The authors declare no competing financial interest.

ACKNOWLEDGEMENTS

The research work of O.S. was supported by Austrian FWF project V279-N19. Authors are very thankful to Dr. Klaudia Hradil (XRC TU Wien) for collaboration.

REFERENCES

(1) Wald, F.; Rosenberg, A. *J. Trans. Metal. Soc. AIME* **1965**, *233*, 796-799.

(2) Aronsson, B.; Stenberg, E.; Åselius, J. *Acta Chem. Scand.* **1960**, *14*, 733-741.

(3) Ellner, M.; Grin, J.; Fischer, P.; Rogl, P. *Z. Metallk.* **1993**, *84*, 788-791.

(4) Samsonov, G.V.; Kosenko, V.A. *Poroshk. Metallurg.* **1971**, *8 (104)*, 25-30.

(5) Hassler, E.; Lundström, T.; Tergenius, L.E. *J. Less-Common Met.* **1979**, *67*, 567-572.

(6) Lanam, R.; Pozarnik, F.; Clal, E.; Volpe, C. Platinum Alloys Characteristics: A Comparison of Existing Platinum Casting Alloys With Pt-Cu-Co, 1997 Platinum Day Symposium, Vol. 3, Platinum Guild International USA, Los Angeles, U.S.A., 1999, http://platinumguild.com/files/pdf/V3N1W_platinum_alloy.pdf.

(7) Jackson, K.M.; Lang, C. *Platinum Metals Rev.* **2006**, *50 (1)*, 15–19.

(8) Hume-Rothery, W.; Smallman, R. W.; Haworth, C. W. The Structure of Metals and Alloys, The Institute of Metals, London, 1969.

(9) Muzzy, L. E.; Avdeev, M.; Lawes, G.; Haas, M. K.; Zandbergen, H.W.; Ramirez, A.P.; Jorgensen, J.D.; Cava, R.J. *Physica C: Superconductivity* **2002**, *382 (2–3)*, 153–165.

(10) Rodriguez-Carvajal, *J. Physica B* **1993**, *192*, 55-69.

(11) Nonius Kappa CCD, Program Package COLLECT, DENZO, SCALEPACK, SORTAV; Nonius Delft, The Netherlands.

(12) Bruker Advanced X-ray Solutions. APEX2 User Manual. Version 1.22, Bruker AXS Inc., 2004.

(13) Bruker. APEXII, SAINT and SADABS., Bruker Analytical X-ray Instruments Inc.: Madison, Wisconsin, USA, 2008.

(14) Sheldrick, G.M. SHELXS-97, Program for the Solution of Crystal Structures, University of Göttingen: Germany, 1997.

(15) Sheldrick, G.M. SHELXL-97, Program for Crystal Structure Refinement, University of Göttingen: Germany, 1997.

(16) Farrugia, L.J. *J. Appl. Cryst.* **1999**, *32*, 837.

(17) Rogl, P.; Nowotny, H.; Benesovsky, F. *Monatsh. Chem.* **1971**, *102*, 678-686.

(18) Lundström, T.; Tergenius, L.E. *Acta Chem. Scand.* **1973**, *27*, 3705-3711.

(19) Parthé, E.; Gelato, L.; Chabot, B.; Penzo, M.; Censual, K.; Gladyshevskii, R. TYPIX – Standardized Data and Crystal Chemical Characterization of Inorganic Structure Types, Springer: Berlin, 1994.

(20) Tergenius, L.E.; Lundström, T. *J. Solid State Chem.* **1980**, *31*, 361-367.

(21) Bever, A.K.V.; Nieuwenkamp, W. *Z. Kristallogr.* **1935**, *90*, 374-376.

(22) Kiessling, R. *Acta Chem. Scand.* **1949**, *3*, 595-602.

(23) Helmholz, L. *Z. Kristallogr., Kristallgeom., Kristallphys., Kristallchem.* **1936**, *95*, 129-137.

(24) Nowotny, H.; Kieffer, R. *Z. Metallkd.* **1947**, *38*, 257-265.

(25) Adam, J.; Rich, J. B. *Acta Cryst.* **1954**, *7*, 813-816.

(26) Jeitschko, W.; Braun, D. *Acta Crystallogr. B* **1977**, *33*, 3401-3406.

(27) Gladyshevskii, R.E.; Grin', Yu.N.; Yarmolyuk, Y.P. *Dopov. Akad. Nauk Ukr. RSR* (Ser. A) **1983**, *2*, 67.

(28) Tkachuk, A.V.; Mar, A. *Inorg. Chem.* **2005**, *44(7)*, 2272-2281.

(29) Gulay, L.D.; Kalychak, Ya.M.; Wolçyrz, M.; Lukaszewicz, K. *J. Alloys Comp.* **2000**, *311*, 238–240.

(30) Massalski, T.B. in Binary Alloy Phase Diagrams, ASM International: Materials Park, OH, 2nd edn., 1990.

(31) Ellner, M. *J. Less-Common Met.* **1981**, *78*, 21-32.

(32) Schneidner, A.; Esch, U. *Z. Electrochem.* **1944**, *50*, 290-301.

(33) Miida, R.; Watanabe, D. *J. Appl. Crystallogr.* **1974**, *7*, 50-59.

(34) Kotur, B.Ya.; Michor, H.; Bauer, E.; Hilscher, G. *J. Alloys Compd.* **2000**, *296 (1-2)*, 285-289.

(35) Gunnarsson, O.; Calandra, M.; Han, J.E. *Rev. Mod. Phys.* **2003**, *75*, 1085.

For Table of Contents Only

Synopsis

A polyhedral view along the *b* axis of the novel binary Pt_2B structure: intergrowth of anti-$CaCl_2$ (A) and boron deficient α-TℓI slabs (B).